Effect of Hydrophobic Groups on Adsorption of Arginine Based Amino Acids to Solid Surfaces in Water

Akinori Fukushima (akinori@u-fukui.ac.jp)
University of Fukui: Fukui Daigaku https://orcid.org/0000-0002-1860-3008
Masaya Hirano
University of Fukui: Fukui Daigaku
Ryuichi Sato
University of Fukui: Fukui Daigaku

Research Article

Keywords: Peptide, Metal surface, Molecular dynamics, Free energy

Posted Date: June 16th, 2022

DOI: https://doi.org/10.21203/rs.3.rs-1644006/v1

Abstract

We calculate the free energies of adsorption between a solid wall and various arginine derivatives in water using molecular dynamics simulations. We vary the hydrophobic group size of the amino acids in two ways and the hydrophilicity of the solid wall in five ways. The free energy of adsorption decreases by increasing the hydrophilicity of the solid wall, regardless of the size of the hydrophobic group. Amino acids with small hydrophobic groups are adsorbed on the solid wall with the strongest hydrophilicity, but the free energy of the amino acids with large hydrophobic groups is relatively small. The free energy of adsorption in benzene solvent is increased by increasing the hydrophilicity of the solid wall; however, analogous to results in water solvent, it is independent of the size of the hydrophobic group. We attribute these differences in free energy to the effect of solvent molecules localized on the solid wall. Thus, these results may modulate peptide adsorption on a solid surface by the size of the peptide's hydrophobic groups.

Introduction

Aptamers are DNA, RNA, and peptides that have a specific affinity for particular substances [1, 2], such as small molecules[3, 4], ions[5, 6], proteins [7, 8], cells [9, 10], and organisms [11, 12]. Although antibodies have similar properties to aptamers, aptamers have many advantages. For example, aptamers are less immunogenic, have better specificity, have higher affinity to their targets, and exhibit less non-specific cross-reactivity than antibodies [13–15]. Because aptamers are selected in vitro, they can be used against a broad range of targets, such as toxic and non-immunogenic substances[16]. Compared with antibodies, aptamers are stable to heat [17] and pH [18], and resistant to organic solvents[19]. Thus, one can select target molecules under non-physiological conditions. Moreover, unlike antibodies, aptamers can undergo several denaturation/refolding cycles without loss of activity[20]. One can mass-produce aptamers by chemical synthesis at low production costs[16]. Accordingly, researchers use aptamers in a broad range of fields, such as diagnostics and therapy[1, 21–25], drug delivery[26–28], and biosensors[29–32].

Sensitive detection of metals based on the affinity and specificity of aptamers is an active field of research in environmental monitoring and medical diagnosis[2]. In medicine, the concentrations of various metals *in vivo* can be used as biomarkers, measurable indicators of biological conditions. For example, titanium and its alloys see use in the production of many medical implants, such as artificial bones and joints. Recent studies suggest that titanium-based implants exhibit wear and corrosion in physiological environments, releasing titanium particles into the surrounding tissues and blood. Because titanium is highly insoluble and can lead to tissue injury, researchers need accurate and facile measurements of the titanium concentration in blood. However, precise measurements require technical equipment, which makes routine monitoring difficult [33]. Using aptamers in blood tests would enable the concentration of various metals in blood, such as titanium, to be measured at a low cost. This would solve the problems associated with conventional testing methods. Thus, it is necessary to develop aptamers with specific and high affinity for various metals.

Numerous peptide aptamers with a specific affinity for various inorganic surfaces has been developed [34–40]. Sano *et al*. identified a peptide TBP-1 (RKLPDAPGMHTW) that specifically binds to Ti by using phage display and suggested that RKLPDA (minTBP-1) in the peptide sequence is pertinent to binding to the Ti surface. Initial studies on the binding affinity suggest that minTBP-1 has affinities for Ti, Si, and Ag; but not for Au, Cr, Pt, Sn, Zn, Cu, and Fe[41]. Regarding the roles of amino acid residues in the minTBP-1 sequence, alanine substitution experiments suggest that mutation of a neutral proline in the sequence decreases these affinities; in contrast, mutation of a charged lysine in the sequence increases them[42]. Skelton *et al*. obtained similar results using molecular dynamics simulations. They suggested that changes in the flexibility of minTBP-1 (due to mutations of proline) and changes in the stability of the molecular structure in the adsorbed state (due to mutations of lysine) are pertinent factors. Furthermore, the interactions of the charged residues in the sequence—Arg, Asp, and Lys—with the water layers structured on the TiO_2 surface drive the initial stage of adsorption of minTBP-1[43]. These results suggest the importance of interfacial water layers in interactions between peptides and TiO_2 surfaces.

Schneider *et al*. performed molecular dynamics simulations to analyze the adsorption of minTBP-1 on TiO_2 and SiO_2 surfaces[44]. Sultan *et al*. suggested that peptide structures and sequences are pertinent to binding affinity, and evaluated various titanium-binding peptides Ti-1 (QPYLFATDSLIK) and Ti-2 (GHTHYHAVRTQT) from the standpoint of entropy and enthalpy. These two peptide sequences differ substantially in terms of the overall balance between hydrophobic and charged residues. Hydropathy scores indicate that Ti-1 has stronger hydrophobicity. However, quartz crystal microbalance experiments show that these two peptides have similar binding affinities for the TiO_2 surface. Molecular dynamics simulations suggest that Ti-1 is an entropically driven binder, with no strong anchor residues, whereas Ti-2 is an enthalpically guided binder, featuring a high number of periodically spaced anchor residues along the chain length[45].

Although many studies have been published on the interactions between biomolecules and inorganic surfaces, researchers still do not fully understand why particular peptides have specific binding affinities for inorganic surfaces. By elucidating the fundamentals of specific recognition between peptides and inorganic surfaces, novel peptide aptamers can be rationally designed on the basis of the properties of the target inorganic surfaces, which will reduce research and development costs. Therefore, it is necessary to understand how the properties of peptides, which are determined by their steric structures and amino acid sequences, affect their interactions with inorganic surfaces and how one can tailor these properties to modulate affinity.

We focused on hydrophobic groups in amino acids to understand their affinity for solid walls. We used virtual amino acid molecules based on arginine. In physiological environments, metal surfaces are oxidized and positively or negatively charged [46]. Assuming a negatively charged metal solid surface, we simulated virtual solid walls with downward dipole moments on the surface. We performed molecular dynamics simulations to evaluate changes in the adsorption states of amino acids and changes in the magnitude of the dipole moments by calculating the free energy.

Computational Details

Figure 1 shows the structures of the virtual amino acids based on arginine used in this study. The amino acid derivatives consist of a hydrophobic carbon chain with an amine that is bonded to the carboxy group of the main chain of arginine, thus constituting an amide bond. The number of carbon atoms in the hydrophobic chain is 1 and 16. We named two carbon atoms in the amino acids. Carbon atoms at the end of the hydrophobic carbon chain are called C_1, and carbons bonded with three hydrogen atoms are called C_2. Figure 2 shows the system used in the simulation and the definition of the reaction coordinate. Figure 2(a) shows the simulation system. The solid wall consists of one virtual atom based on FCC's crystal structure. The orientation of the surface where the virtual molecules adsorb is the (111) plane. We prepared a supercell volume, 39.0 Å×29.4 Å×300 Å. For solvent molecules, we used 5000 water molecules. The number of virtual molecules was one. We used periodic boundary conditions in all directions. Figure 2(b) shows the schematic diagram of the reaction path. We employed a difference of the z-coordinate between the surface of the solid wall and the center of mass of the amino acid.

We determined the partial atomic charge of the amino acids by fitting the electron density calculated from optimized structures using the restrained electrostatic potential method. All electronic structure calculations were carried out on the basis of the density functional theory using Gaussian16[47]. We used B3LYP[48] functionals as the exchange-correlation functionals. Moreover, the 6-31G** basis set was used for all atoms. We used harmonic oscillators for the bond, angle, and dihedral potentials. The SPC/E[49] model was used for water molecules and the General Amber Force Field[50] for the amino acid. We evaluated interaction parameters between various atoms using the Lorentz–Berthelot mixing rule. We set the Coulomb and Lennard–Jones potential cutoffs at 10 Å and the dipole potential cutoff at 15 Å. The particle–particle-particle–mesh methods[51] were used to calculate the distance beyond the cutoff distance of the Coulomb potential. We constrained the bond lengths and bond angles of the water molecules by the SHAKE[52] method.

To maintain the structure of the solid wall, we used a harmonic oscillator potential between virtual atoms in the unit cell (Fig. 2):

$$\phi_{Harmonic} = K(r - r_0)^2 \qquad (1)$$

where r is the distance to atoms, r_0 is the equilibrium distance between two atoms (4.08 Å), and K is a constant (500 kcal/mol/Å^2). Assuming a negatively charged surface, all atoms in the outermost layers were assigned downward dipole moments in the simulation. We changed the magnitude of the dipole moment (D) to 0.0 eÅ, 0.5 eÅ, 1.0 eÅ, 1.5 eÅ, and 2.0 eÅ. To represent the electric field on the solid wall by this dipole moment, the charges of all the atoms constituting the solid wall were assumed to be zero. We set the parameters ε and σ of the virtual atoms of the solid walls to appropriate values to prevent solvent molecules from entering the solid wall.

We carried out molecular dynamics simulations with LAMMPS[53]. In the initial state, virtual molecules were placed at a distance of 10 Å from the solid wall surface to its center of mass, and water molecules

were randomly placed in the region of 25–100 Å from the solid wall surface. We set the time step for the numerical integration to 1 fs. We calculated the free energy using the umbrella sampling method [54] and the weighted histogram analysis method[55]. In this study, the reaction coordinates were defined as the distance from the solid wall surface (z_w) to the center of gravity of the amino acid (z_p), as shown in Fig. 2(b). We varied the reaction coordinates from 4.8 Å to 22.8 Å in increments of 1.0 Å up to the bulk solvent. To control the reaction coordinates, a harmonic potential was imposed to constrain only the distance in the z-direction, leaving the amino acids free to move in the *xy* direction.

At the first step of the simulation, to create a stable state constrained by the harmonic potential, we set the spring constant for the harmonic potential to control the reaction coordinate to 1000 kcal/mol/Å^2 and calculated 200 ps in the *NVT* ensemble at a temperature of 300 K. Then, we changed the spring constant to 100 kcal/mol/Å^2, and ran the simulation for 200 ps. After obtaining the equilibrium state, we set the spring constant for the harmonic potential to control the reaction coordinate to 1 kcal/mol/Å^2 and performed the calculation for 200 ps for sampling.

Results And Discussion

First, we will discuss the adsorption free energy. The free energy at each reaction coordinate is shown in Fig. 3. Figure 3(a) shows the free energy of the amino acid with $n = 1$, and Fig. 3(b) shows the free energy of the amino acid with $n = 16$. The red line indicates results in the case of $D = 0$ *e*Å, the green line those for $D = 0.5$ *e*Å, the blue line those for $D = 1.0$ *e*Å, the purple line those for $D = 1.5$ *e*Å, and the black line those for $D = 2.0$ *e*Å. The free energy at $z = 22.8$ Å was set to 0, where the amino acid was sufficiently far from the solid wall to ignore the interaction between the amino acid and the solid wall. The horizontal axis shows the reaction path of the amino acid. For $n = 1$, the free energy curve can be divided into two types. One type can be seen when the dipole moment is 0 *e*Å, 0.5 *e*Å, and 1 *e*Å. In this type, the stable point is located where the distance parameter is 5 Å. However, for dipole moments of 1.5 *e*Å and 2.0 *e*Å, there is an adsorption point near 7 Å (the local stable state in 2.0 *e*Å). These different adsorption points indicate that the adsorption state may change with the magnitude of the dipole moment. Even when n is 16, the free energy curve can be divided into two parts. One is the type with adsorption points in the region near 5 Å, as in the case of $n = 1$ ($D = 0$ *e*Å, 0.5 *e*Å, 1.0 *e*Å), and the other is the type with adsorption points in the area farthest from the wall ($D = 1.5$ *e*Å, 2.0 *e*Å).

Figure 4 shows the magnitude of the free energy of the adsorbed state at each dipole for the amino acid with $n = 1$ and $n = 16$. When the dipole is 0 *e*Å, the adsorption energy increases in proportion to the number of carbons in the virtual molecule. However, as the dipole increases, the magnitude of the adsorption free energy of the virtual molecule with $n = 16$ becomes smaller than that of the amino acids with $n = 1$. This indicates that the decrease in the magnitude of the free energy is dependent on the size of the hydrophobic component of the amino acid. However, the rate of increase in adsorption free energy of $n = 16$ amino acids with the sizeable hydrophobic component is more significant than that of the $n = 1$ amino acids. This indicates that the adsorption on the solid wall can be regulated by adjusting the size of the hydrophobic component.

Next, we discuss adsorption geometry. We focus on the difference of the stable structure and the magnitude of the dipole moment. Figure 5 shows the probability distribution of two carbon atoms. Figure 5(a) indicates results of $n = 1$, and Fig. 5(b) indicates results of $n = 16$. We defined the distance between carbon atom C_1 at the bonded end of the side chain of arginine and the solid wall and the distance between the free terminus carbon atom C_2 at the end of the hydrophobic component of the amino acid and the solid wall as parameters as shown in Fig. 1. The horizontal axis shows the parameters defined above and the vertical axis represents the probability distribution. Purple lines indicate results of C_1 and red lines indicate results of C_2. Moreover, solid lines indicate results of $D = 0$ *e*Å and dashed lines indicate results of $D = 2$ *e*Å. In the case of $n = 1$, comparing the case of $D = 0$ *e*Å with the case of $D = 2$ *e*Å, we can see that the position of C_2 does not change, but the position of C_1 differs significantly. This indicates that when D is equal to 0 *e*Å, the molecule is parallel to the solid wall, while when D is equal to 2 *e*Å, the molecule is perpendicular to the solid wall. We also show the schematic diagram of the adsorption structure at $n = 1$ in Fig. 6. Figure 6(a) indicates that the molecule is parallel to the solid wall ($D = 0$ *e*Å), and Fig. 6(b) indicates that the molecule is perpendicular to the solid wall ($D = 2$ *e*Å). As shown in Fig. 6(a), when the dipole moment of the solid wall is zero, because the molecule is adsorbed on the solid wall via the non-coulombic interaction, atoms that compose the molecule are adsorbed in a state where the distance between them and the solid wall becomes small. However, in the case of the $D = 2$ *e*Å, the dipole interacts strongly with charged atoms such as oxygen in water, and nitrogen in the molecule. As a result, carbon atoms, which have fewer charges, are inhibited by water to close the solid wall. This fact indicates that the adsorption of amino acids on solid walls in water is likely to be determined by the magnitude of the interaction between the solid surface and water molecules and charged sites such as nitrogen atoms, i.e., the size of the surface dipole, and the length of the carbon chain with which these interactions are small.

Conclusions

We focused on the effect of hydrophobic groups in amino acid molecules to obtain fundamental insight into modulating the peptide binding affinity to solid walls. We modeled amino acids with different-sized hydrophobic groups based on arginine, a polar amino acid with a high affinity for inorganic surfaces. To investigate the effect of the difference of the surface dipole on the adsorption free energy, we simulated a solid wall with a downward dipole moment on the surface. We performed molecular dynamics simulations to evaluate the change in the adsorption state of amino acids and the free energy due to the difference in the dipole moment on the solid wall. As the dipole moment of the solid surface was increased, the free energy of the amino acid adsorption decreased regardless of the size of the hydrophobic group. Still, the increasing rate of the free energy of the $n = 1$ amino acid was more significant than that of the $n = 16$ amino acid. As a result, when the magnitude of the dipole moment is greater than 1 *e*Å, the free energy of the amino acid with a large hydrophobic group will be smaller than that of an amino acid with a small hydrophobic group. This result suggests that the adsorption state may be controlled by the size of the hydrophobic group. Next, we focused on the adsorption geometry of the amino acid. In the case of $n = 1$, when D is smaller than 1 *e*Å, the amino acid is adsorbed parallel to the

solid wall. However, when D is higher than 1.5 eÅ, the amino acid is adsorbed perpendicular to the solid wall. This difference is caused by the coulombic interaction between water molecules and the solid wall. This fact indicates that the adsorption of amino acids on solid walls in water is likely to be determined by the magnitude of the interaction between the solid surface and water molecules and charged sites such as nitrogen atoms, i.e., the size of the surface dipole, and the length of the carbon chain for which these interactions are small.

Declarations

Acknowledgments

In this research work, we used the supercomputer of ACCMS, Kyoto University.

Ethics declarations

Funding

This work was not supported by any funding.

Competing Interests

The authors declare that no competing interests.

Data Availability

All data will be available on reasonable request.

Code availability

Not applicable.

Author Contributions

Akinori Fukushima and Masaya Hirano performed the simulation and the data analysis and wrote a part of the article. Ryuichi Sato performed the simulation and the data analysis. All authors contributed to the general discussion.

References

1. Kadioglu O, Efferth T (2016) Peptide aptamer identified by molecular docking targeting translationally controlled tumor protein in leukemia cells. Invest New Drugs 34:515–521. https://doi.org/10.1007/s10637-016-0339-6

2. Farzin L, Shamsipur M, Sheibani S (2017) A review: Aptamer-based analytical strategies using the nanomaterials for environmental and human monitoring of toxic heavy metals. Talanta 174:619–627. https://doi.org/https://doi.org/10.1016/j.talanta.2017.06.066
3. Shamsipur M, Farzin L, Tabrizi MA, Shanehsaz M (2016) CdTe amplification nanoplatforms capped with thioglycolic acid for electrochemical aptasensing of ultra-traces of ATP. Mater Sci Eng C 69:1354–1360. https://doi.org/https://doi.org/10.1016/j.msec.2016.08.038
4. Zhang S, Wang L, Liu M et al (2016) A novel, label-free fluorescent aptasensor for cocaine detection based on a G-quadruplex and ruthenium polypyridyl complex molecular light switch. Anal Methods 8:3740–3746. https://doi.org/10.1039/C6AY00231E
5. Zhou W, Ding J, Liu J (2017) 2-Aminopurine-modified DNA homopolymers for robust and sensitive detection of mercury and silver. Biosens Bioelectron 87:171–177. https://doi.org/https://doi.org/10.1016/j.bios.2016.08.033
6. Guo Y, Chen Y, Wei Y et al (2015) Label-free fluorescent aptasensor for potassium ion using structure-switching aptamers and berberine. Spectrochim Acta Part A Mol Biomol Spectrosc 136:1635–1641. https://doi.org/https://doi.org/10.1016/j.saa.2014.10.058
7. Amouzadeh Tabrizi M, Shamsipur M, Farzin L (2015) A high sensitive electrochemical aptasensor for the determination of VEGF165 in serum of lung cancer patient. Biosens Bioelectron 74:764–769. https://doi.org/https://doi.org/10.1016/j.bios.2015.07.032
8. Shamsipur M, Farzin L, Tabrizi MA (2016) Ultrasensitive aptamer-based on-off assay for lysozyme using a glassy carbon electrode modified with gold nanoparticles and electrochemically reduced graphene oxide. Microchim Acta 183:2733–2743. https://doi.org/10.1007/s00604-016-1920-6
9. Mir TA, Yoon J-H, Gurudatt NG et al (2015) Ultrasensitive cytosensing based on an aptamer modified nanobiosensor with a bioconjugate: Detection of human non-small-cell lung cancer cells. Biosens Bioelectron 74:594–600. https://doi.org/https://doi.org/10.1016/j.bios.2015.07.012
10. Wang T, Liu J, Gu X et al (2015) Label-free electrochemical aptasensor constructed by layer-by-layer technology for sensitive and selective detection of cancer cells. Anal Chim Acta 882:32–37. https://doi.org/https://doi.org/10.1016/j.aca.2015.05.008
11. Labib M, Zamay AS, Kolovskaya OS et al (2012) Aptamer-Based Viability Impedimetric Sensor for Bacteria. Anal Chem 84:8966–8969. https://doi.org/10.1021/ac302902s
12. Labib M, Zamay AS, Muharemagic D et al (2012) Aptamer-Based Viability Impedimetric Sensor for Viruses. Anal Chem 84:1813–1816. https://doi.org/10.1021/ac203412m
13. Collett JR, Cho EJ, Ellington AD (2005) Production and processing of aptamer microarrays. Methods 37:4–15. https://doi.org/https://doi.org/10.1016/j.ymeth.2005.05.009
14. Mayer G (2009) The Chemical Biology of Aptamers. Angew Chemie Int Ed 48:2672–2689. https://doi.org/https://doi.org/10.1002/anie.200804643
15. Templin MF, Stoll D, Schrenk M et al (2002) Protein microarray technology. Trends Biotechnol 20:160–166. https://doi.org/https://doi.org/10.1016/S0167-7799(01)01910-2

16. Kadioglu O, Malczyk AH, Greten HJ, Efferth T (2015) Aptamers as a novel tool for diagnostics and therapy. Invest New Drugs 33:513–520. https://doi.org/10.1007/s10637-015-0213-y
17. Langer R (1998) Drug delivery and targeting. Nature 392:5–10
18. Farokhzad OC, Cheng J, Teply BA et al (2006) Targeted nanoparticle-aptamer bioconjugates for cancer chemotherapy in vivo. Proc Natl Acad Sci 103 6315 LP – 6320. https://doi.org/10.1073/pnas.0601755103
19. Wilson C, Szostak JW (1998) Isolation of a fluorophore-specific DNA aptamer with weak redox activity. Chem Biol 5:609–617. https://doi.org/https://doi.org/10.1016/S1074-5521(98)90289-7
20. Liss M, Petersen B, Wolf H, Prohaska E (2002) An Aptamer-Based Quartz Crystal Protein Biosensor. Anal Chem 74:4488–4495. https://doi.org/10.1021/ac011294p
21. Han J, Gao L, Wang J, Wang J (2020) Application and development of aptamer in cancer: from clinical diagnosis to cancer therapy. J Cancer 11:6902–6915. https://doi.org/10.7150/jca.49532
22. Nimjee SM, Rusconi CP, Sullenger BA (2004) Aptamers: An Emerging Class of Therapeutics. Annu Rev Med 56:555–583. https://doi.org/10.1146/annurev.med.56.062904.144915
23. Xing H, Hwang K, Li J et al (2014) DNA aptamer technology for personalized medicine. Curr Opin Chem Eng 4:79–87. https://doi.org/https://doi.org/10.1016/j.coche.2014.01.007
24. Kanwar JR, Shankaranarayanan JS, Gurudevan S, Kanwar RK (2014) Aptamer-based therapeutics of the past, present and future: from the perspective of eye-related diseases. Drug Discov Today 19:1309–1321. https://doi.org/https://doi.org/10.1016/j.drudis.2014.02.009
25. Santosh B, Yadava PK (2014) Nucleic acid aptamers: research tools in disease diagnostics and therapeutics. Biomed Res Int 2014:540451. https://doi.org/10.1155/2014/540451
26. Wang C, Liu B, Lu J et al (2014) Strategies for combination of aptamer and targeted drug delivery. J Nanosci Nanotechnol 14:501–512. https://doi.org/10.1166/jnn.2014.8746
27. Zhou J, Rossi JJ (2014) Cell-type-specific, Aptamer-functionalized Agents for Targeted Disease Therapy. Mol Ther - Nucleic Acids 3:e169. https://doi.org/https://doi.org/10.1038/mtna.2014.21
28. Xiang D, Shigdar S, Qiao G et al (2015) Nucleic acid aptamer-guided cancer therapeutics and diagnostics: the next generation of cancer medicine. Theranostics 5:23–42. https://doi.org/10.7150/thno.10202
29. Kim YS, Gu MB (2014) Advances in aptamer screening and small molecule aptasensors. Adv Biochem Eng Biotechnol 140:29–67. https://doi.org/10.1007/10_2013_225
30. MacKay S, Wishart D, Xing JZ, Chen J (2014) Developing Trends in Aptamer-Based Biosensor Devices and Their Applications. IEEE Trans Biomed Circuits Syst 8:4–14. https://doi.org/10.1109/TBCAS.2014.2304718
31. Zhou W, Huang P-JJ, Ding J, Liu J (2014) Aptamer-based biosensors for biomedical diagnostics. Analyst 139:2627–2640. https://doi.org/10.1039/c4an00132j
32. Reverdatto S, Burz DS, Shekhtman A (2015) Peptide aptamers: development and applications. Curr Top Med Chem 15:1082–1101. https://doi.org/10.2174/1568026615666150413153143

33. Swiatkowska I, Martin N, Hart AJ (2019) Blood titanium level as a biomarker of orthopaedic implant wear. J trace Elem Med Biol organ Soc Miner Trace Elem 53:120–128. https://doi.org/10.1016/j.jtemb.2019.02.013
34. Brown S (1992) Engineered iron oxide-adhesion mutants of the Escherichia coli phage lambda receptor. Proc Natl Acad Sci U S A 89:8651–8655. https://doi.org/10.1073/pnas.89.18.8651
35. Brown S (1997) Metal-recognition by repeating polypeptides. Nat Biotechnol 15:269–272. https://doi.org/10.1038/nbt0397-269
36. Whaley SR, English DS, Hu EL et al (2000) Selection of peptides with semiconductor binding specificity for directed nanocrystal assembly. Nature 405:665–668. https://doi.org/10.1038/35015043
37. Naik RR, Stringer SJ, Agarwal G et al (2002) Biomimetic synthesis and patterning of silver nanoparticles. Nat Mater 1:169–172. https://doi.org/10.1038/nmat758
38. Sarikaya M, Tamerler C, Jen AK-Y et al (2003) Molecular biomimetics: nanotechnology through biology. Nat Mater 2:577–585. https://doi.org/10.1038/nmat964
39. Kjærgaard K, Sørensen JK, Schembri MA, Klemm P (2000) Sequestration of Zinc Oxide by Fimbrial Designer Chelators. Appl Environ Microbiol 66. https://doi.org/10.1128/AEM.66.1.10-14.2000. :10 LP – 14
40. Naik RR, Brott LL, Clarson SJ, Stone MO (2002) Silica-precipitating peptides isolated from a combinatorial phage display peptide library. J Nanosci Nanotechnol 2:95–100. https://doi.org/10.1166/jnn.2002.074
41. Lee S-W, Mao C, Flynn CE, Belcher AM (2002) Ordering of quantum dots using genetically engineered viruses. Science 296:892–895. https://doi.org/10.1126/science.1068054
42. Sano K-I, Sasaki H, Shiba K (2005) Specificity and Biomineralization Activities of Ti-Binding Peptide-1 (TBP-1). Langmuir 21:3090–3095. https://doi.org/10.1021/la047428m
43. Sano K-I, Shiba K (2003) A Hexapeptide Motif that Electrostatically Binds to the Surface of Titanium. J Am Chem Soc 125:14234–14235. https://doi.org/10.1021/ja038414q
44. Skelton AA, Liang T, Walsh TR (2009) Interplay of Sequence, Conformation, and Binding at the Peptide – Titania Interface as Mediated by Water. ACS Appl Mater Interfaces 1:1482–1491. https://doi.org/10.1021/am9001666
45. Schneider J, Ciacchi LC (2012) Specific material recognition by small peptides mediated by the interfacial solvent structure. J Am Chem Soc 134:2407–2413. https://doi.org/10.1021/JA210744G
46. Sultan AM, Westcott ZC, Hughes ZE et al (2016) Aqueous Peptide–TiO2 Interfaces: Isoenergetic Binding via Either Entropically or Enthalpically Driven Mechanisms. ACS Appl Mater Interfaces 8:18620–18630. https://doi.org/10.1021/acsami.6b05200
47. Kosmulski M (2016) Isoelectric points and points of zero charge of metal (hydr)oxides: 50years after Parks' review. Adv Colloid Interface Sci 238:1–61. https://doi.org/https://doi.org/10.1016/j.cis.2016.10.005

48. Frisch MJ et al (2016)Gaussian09
49. Becke AD (1993) Density-functional thermochemistry. III. The role of exact exchange. J Chem Phys 98:5648–5652. https://doi.org/10.1063/1.464913
50. Berendsen HJC, Grigera JR, Straatsma TP (1987) The missing term in effective pair potentials. J Phys Chem 91:6269–6271
51. Wang J, Wolf RM, Caldwell JW et al (2004) Development and testing of a general amber force field. J Comput Chem 25:1157–1174. https://doi.org/https://doi.org/10.1002/jcc.20035
52. Hockney RW, Eastwood JW (1966) Computer simulation using particles
53. Ryckaert JP, Ciccotti G, Berendsen HJC (1977) Numerical Integration of the Cartesian Equations of Motion of a System with Constraints: Molecular Dynamics of n-Alkanes. J Comput Phys 23:327–341. https://doi.org/10.1016/0021-9991(77)90098-5
54. Plimpton S (1995) Fast parallel algorithms for short-range molecular dynamics. J Comput Phys 117:1–19
55. Frenkel D, Smit B (2002) Understanding Molecular Simulation, 2nd edn. Academic Press, San Diego
56. Grossfield A “WHAM: the weighted histogram analysis method”, version 2.0.11. http://membrane.urmc.rochester.edu/wordpress/?page_id=126
57. **Ethics declarations**

Figures

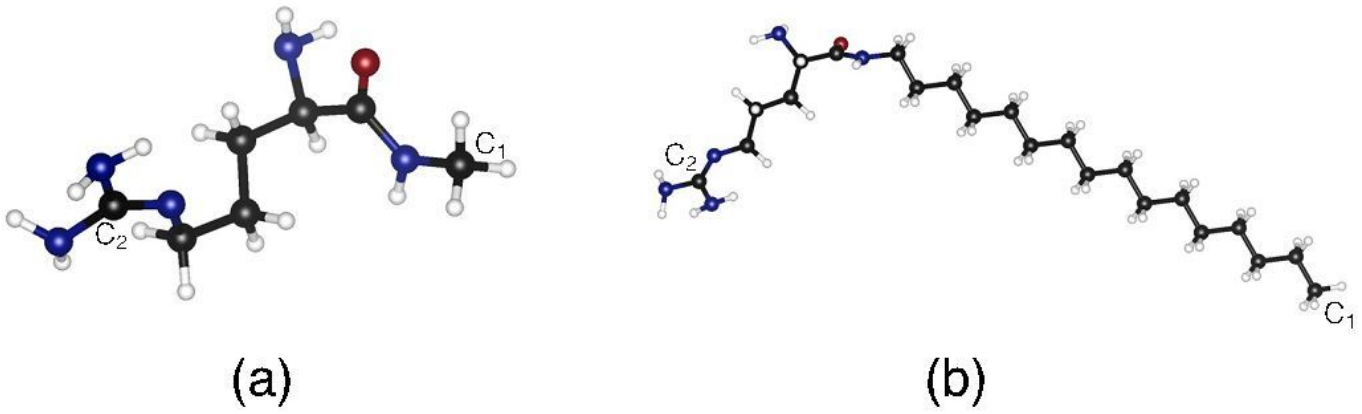

Figure 1

Chemical structures of molecules used in this study: (a) $n = 1$; (b) $n = 16$.

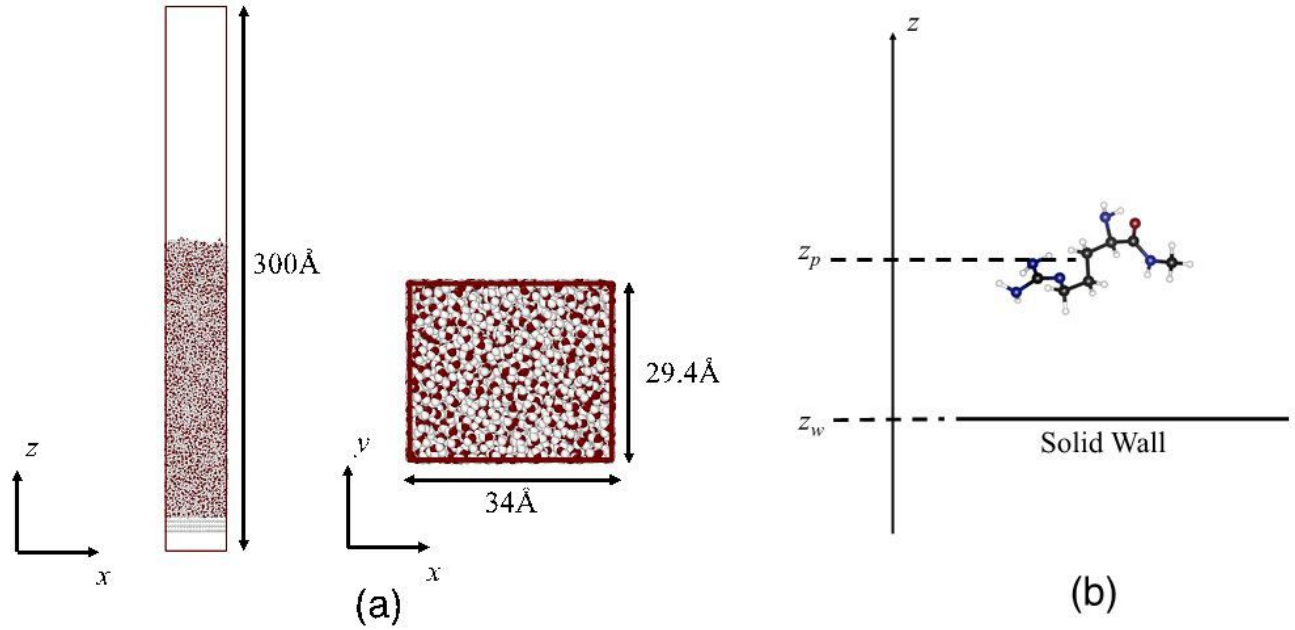

Figure 2

Simulation systems and wall structures used in this study: (a) simulation system; (b) reaction pathway.

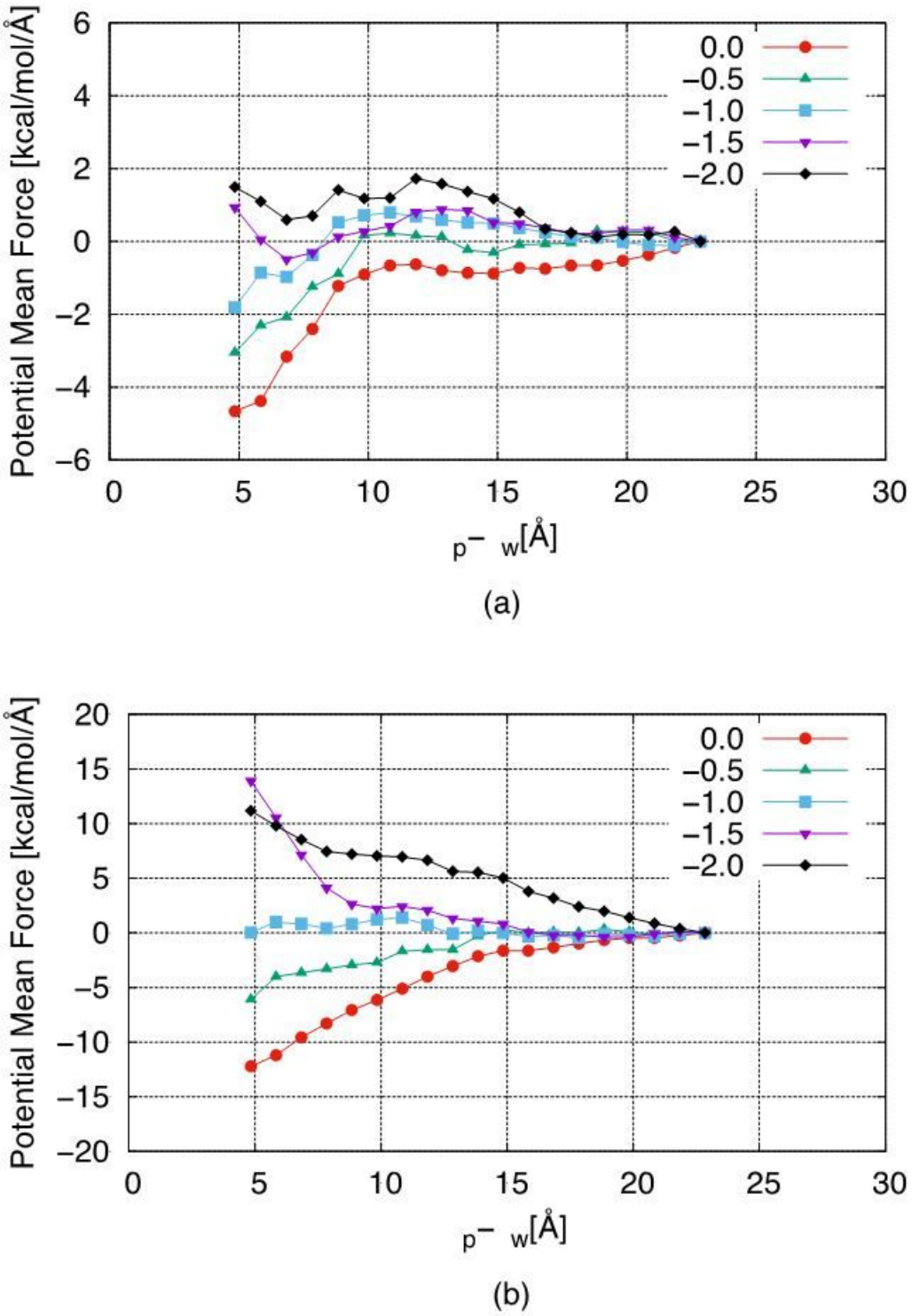

Figure 3

Free energy diagram along the reaction path: (a) n = 1; (b) n = 16.

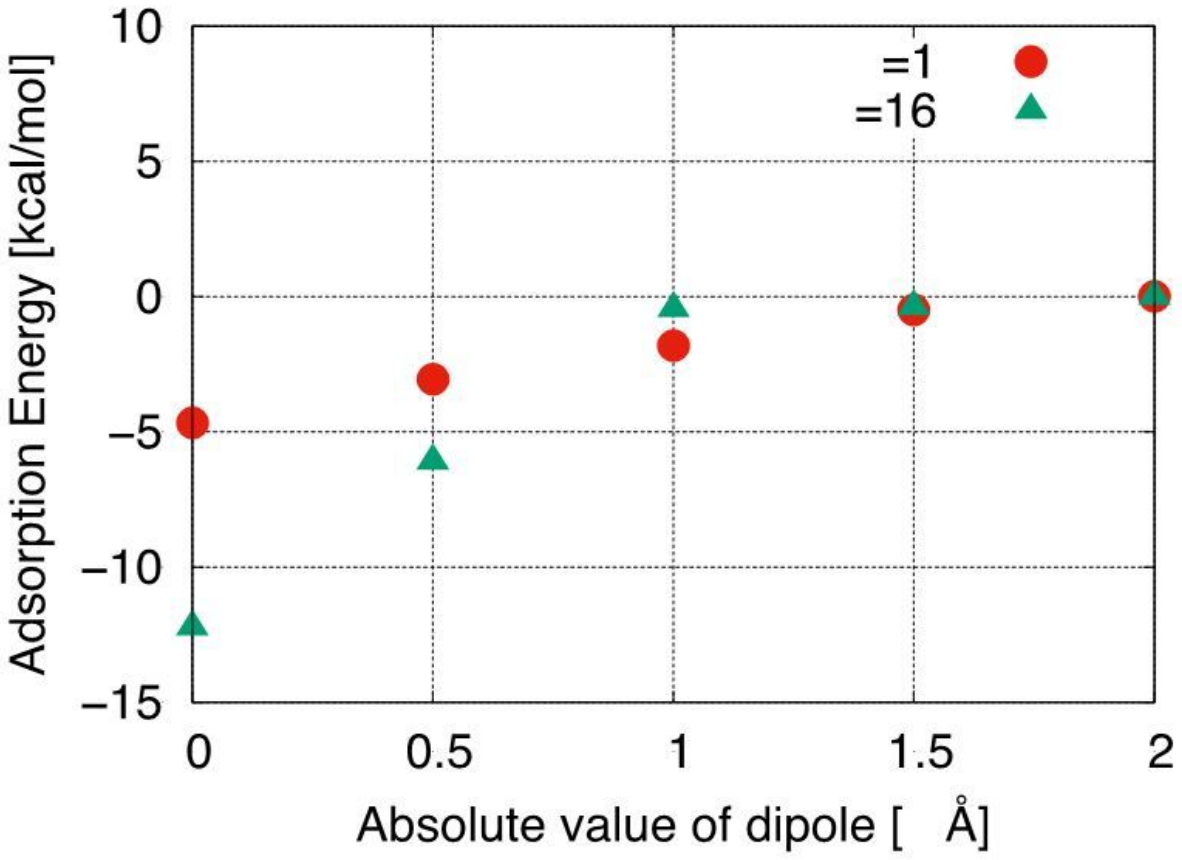

Figure 4

Dependence of the adsorption free energy on the magnitude of the dipole moment. Red, *n* = 1; purple, *n* = 16.

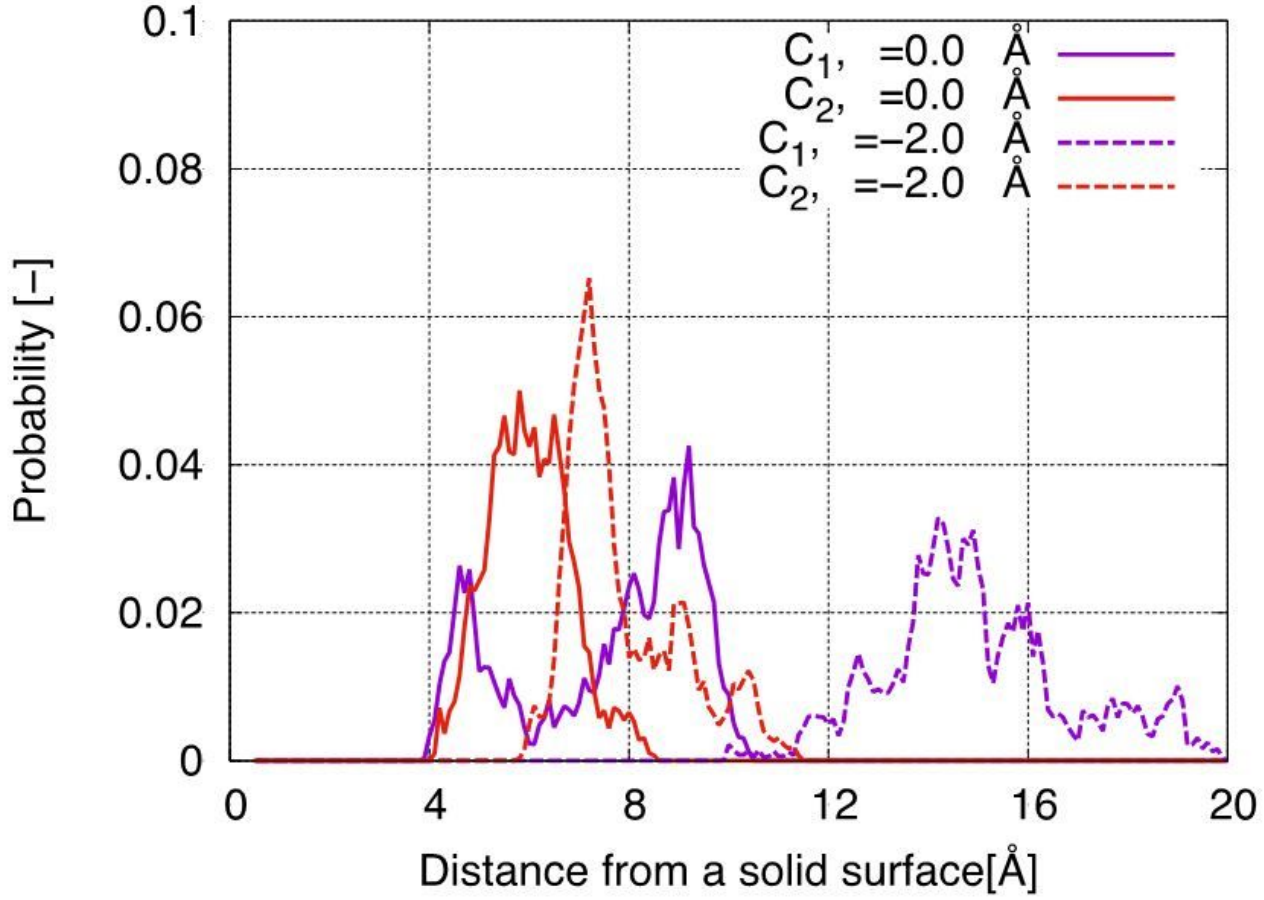

Figure 5

Probability density distributions: (a) $n = 1$; (b) $n = 16$.

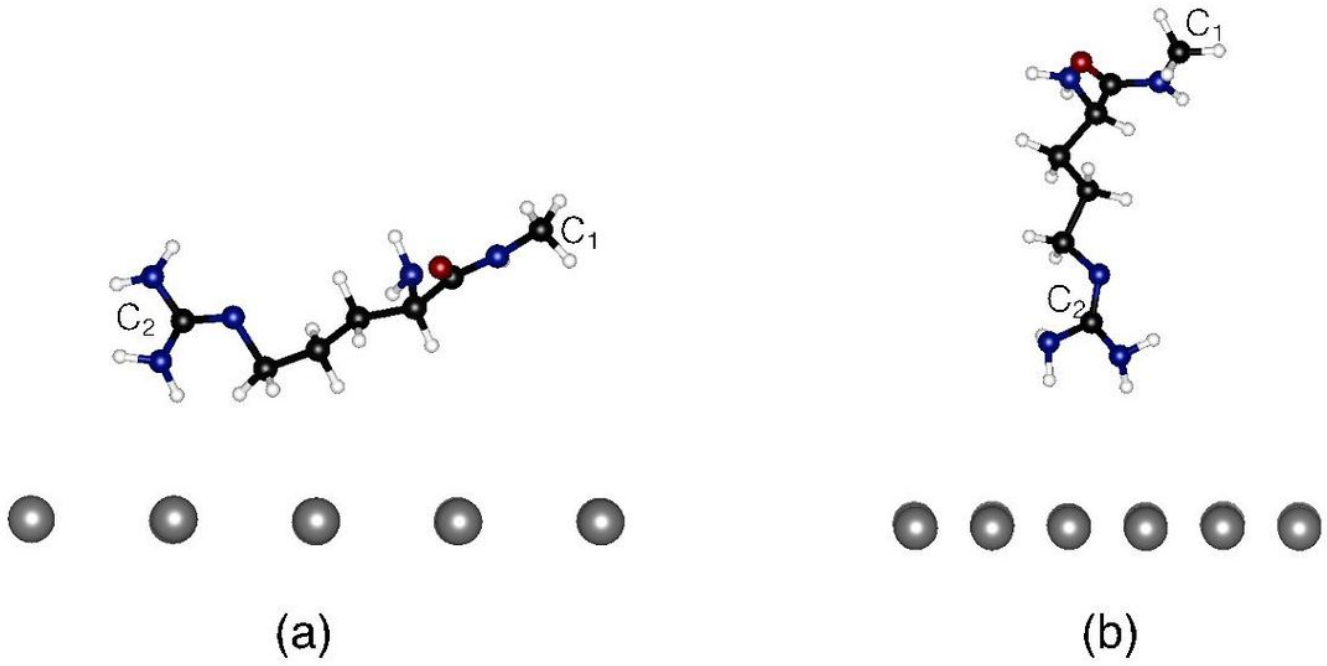

Figure 6

Schematic illustration of the adsorbed amino acid on the solid wall: (a) stable structure for n = 1, D = 0 eÅ; (b) local minimum structure for n = 1, D = 2 eÅ.